A Geometric Calibration Method for an Open Cone-Beam CT System

Fabian Stopp, Adam J. Wieckowski, Marc Käseberg, Sebastian Engel, Felix Fehlhaber, Erwin Keeve

***Abstract*—The image quality of cone-beam CT systems depends directly on the precise knowledge of position and orientation of the X-ray source and the detector. The current methods to determine this geometric information are mainly focused on conventional cone-beam CTs with planar or near-planar scanning trajectories. Due to the fixed alignment of X-ray source and detector, such systems have disadvantages in intraoperative use.**

Therefore, we develop a first prototype for cone-beam CT characterized by a free alignment of X-ray source and detector. This results in an open system allowing an intraoperative access to the patient and the implementation of non-planar scanning trajectories in the operating room.

In this paper, we present a geometric calibration method to determine the position and orientation of X-ray source and detector for any arbitrary projection. Enhancing the theoretical method proposed in Mennessier et al. [1] by introducing an asymmetrical marker arrangement, we realized a calibration method suitable for practical use. We analyzed the resulting accuracy and applied our approach to the open cone-beam CT prototype.

***Index Terms*—Computed tomography, cone-beam, geometric calibration, non-planar scanning trajectories.**

I. Introduction

In cone-beam computed tomography (CBCT) an object can be three-dimensionally (3D) reconstructed by acquiring X-ray images of this object from different directions. Conventional CBCT systems are characterized by a rigid configuration of X-ray source and image detector, mostly fixed on a C-shaped arm or inside a closed gantry. For 3D image acquisition, source and detector are rotating on a planar trajectory around the patient. With such systems a high image quality is achievable, but the intraoperative use during surgery can be time consuming and complicated. Due to the fixed arrangement of X-ray source and image detector on opposite sides, the patient is surrounded by the system setup and the access for the surgeon is restricted. Therefore, we develop a first experimental open CBCT system for interventional surgery (ORBIT, fig. 1 and 2). The X-ray source is fixed on a robot-arm and the digital flat-panel detector is mounted on a self-constructed motorized mechanism directly connected to the patient table. This system allows a free alignment of X-ray source and image detector towards the patient and offers new opportunities for non-planar scanning trajectories (e.g. fig. 2).

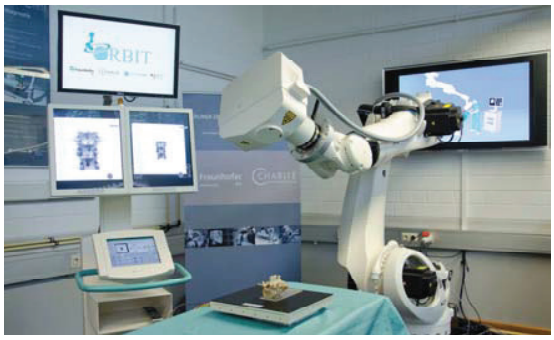

Fig. 1. Current prototype of the open cone-beam CT system (ORBIT) consisting of a pulsed X-ray source (Ziehm Vision R 20 kW) on a robot arm (Kuka KR 150 R2700 extra) and a currently fixed flat-panel detector (Varian PaxScan 3030+).

The essential precondition for CBCT is the knowledge of the exact projection geometry of each acquired image. Therefore the position of the focal spot of the X-ray source and the position and orientation of the X-ray image detector is needed. This information, described by nine parameters, can be determined by a geometric calibration. Most of the available calibration methods use dedicated objects with a known geometric configuration of small balls of high attenuation. By acquiring X-ray images of these objects and identifying the ball projections, the needed parameters of each single image can be determined. But the majority of proposed methods were developed for conventional CBCT systems with planar or near-planar scanning trajectories (e.g. in [2]-[7]). Other approaches without constraints on the scanning trajectory or the alignment of source and detector use complex numerical optimization techniques, e.g. in [8]. In [1] a fully analytical calibration method for near-planar trajectories (using a six points calibration phantom) and for arbitrary scanning trajectories (using a 14 points calibration phantom) were introduced and first simulated results were shown. In further work the direct calibration method for near-planar trajectories was realized and applied to an isocentric c-arm X-ray system using a 6 balls calibration object [9].

Based on the work presented in Mennessier et al. [1], we developed, applied and evaluated a direct geometric

This work is funded by the German Federal Mininstry of Education and Research (BMBF), research grant 13EZ1115A-C.

F. Stopp and Prof. Dr. E. Keeve are with the Department of Maxillofacial Surgery and Clinical Navigation, Charité – Universitätsmedizin Berlin, Augustenburger Platz 1, 13353 Berlin, Germany (e-mail: keeve@charite.de).

A. J. Wieckowski, M. Käseberg, S. Engel, F. Fehlhaber and Prof. Dr. E. Keeve are with the Fraunhofer-Institute for Production Systems and Design Technology IPK, Pascalstrasse 8-9, 10587 Berlin, Germany.

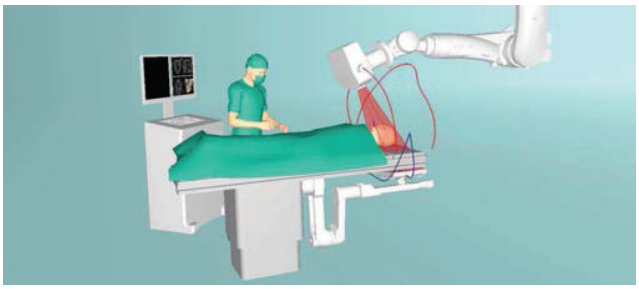

Fig. 2. Open cone-beam CT system ORBIT with an X-ray source fixed on a ceiling-mounted robot arm and a robot-guided flat panel detector directly connected with the patient table. The red path and the blue path indicate an exemplary non-planar scanning trajectory of the X-ray source and detector.

calibration method with a subsequent optimization of the parameters for arbitrary scanning trajectories. In contrast to the simulations in [1], no additional features of the calibration markers are used for marker identification, like absorption coefficients or marker size. After first simulation results, we applied our calibration method to the open CBCT prototype.

II. Our Geometric Calibration Method

To calibrate and determine the nine geometric parameters of an arbitrary image acquisition (X-ray source position, image position and image orientation), we defined the marker arrangement of the calibration object.

A. Marker arrangement

Similar to [1], we align four ball markers on each of the three orthogonal axes and two additional markers on the diagonal axis ($\mathbf{x}_1..\mathbf{x}_4$, $\mathbf{y}_1..\mathbf{y}_4$, $\mathbf{z}_1..\mathbf{z}_4$, $\mathbf{s}_1$, $\mathbf{s}_2$). For the marker assignment to be independent of additional marker features, like size or X-ray absorption coefficients, we defined five constants K_1, K_2, α_x, α_y, and α_z and modified the arrangement of $M = 14$ ball markers (fig. 3). The arrangement of the four markers on the x-axis is:

$$\begin{aligned} \mathbf{x}_1 &= -\alpha_x K_1 \mathbf{e}_x & \mathbf{x}_2 &= -K_1 \mathbf{e}_x \\ \mathbf{x}_3 &= K_2 \mathbf{e}_x & \mathbf{x}_4 &= \alpha_x K_2 \mathbf{e}_x \end{aligned} \tag{1}$$

The arrangement of the eight markers on the y- and z-axis (using α_y and α_z) is equivalent to (1). The three unit vectors $\mathbf{e}_x$, $\mathbf{e}_y$ and $\mathbf{e}_z$ represent the axes of the calibration object's coordinate system. The two diagonal markers are aligned as follows:

$$\mathbf{s}_1 = -K_1(\mathbf{e}_x + \mathbf{e}_y + \mathbf{e}_z) \quad \mathbf{s}_2 = K_2(\mathbf{e}_x + \mathbf{e}_y + \mathbf{e}_z) \tag{2}$$

Depending on the system characteristics of our open CBCT setup (image size of 298 x 298 mm² and a cone-beam opening angle of 16°), we used the following values: $K_1 = 25$ mm, $K_2 = 35$ mm and $\alpha_x = 1.4$, $\alpha_y = 1.7$, and $\alpha_z = 2$. These constants fulfill our basic precondition for good calibration results: the 14 marker must be fully contained and fill as much as possible of the X-ray image.

B. Marker detection

To detect the regions of the projected ball markers in the X-ray images, we apply the following four steps:

1. Segmenting the regions of the ball marker projections by an adaptive threshold.
2. Classification of the segmented regions.
3. Analyzing the blob response of the region using the determinant of Hessian.
4. Analyzing the foreground to background intensity difference.

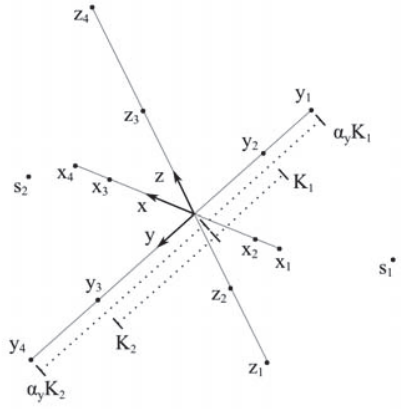

Fig. 3. The arrangement of the 14 ball markers of the calibration object. Four markers are placed on each orthogonal axis and two on the diagonal. The exact positions are defined by the constants K_1, K_2 and α_x, α_y, and α_z.

A region is described by a set of N pixel positions $\mathbf{r}_k$ and intensities I_k. Given the neighborhood of that region with a mean intensity of background b, the projection of the marker center is estimated as the center of mass with background suppression [10]:

$$\mathbf{d} = \left(\sum_{k=1}^{N} (I_k - b) \cdot \mathbf{r}_k \Big/ \sum_{k=1}^{N} (I_k - b) \right) \tag{3}$$

In the following section, we assume that all 14 marker projections are detected in the image. The degenerated cases (e.g. marker overlaps) are described in section II E.

C. Marker assignment

We divide the detected marker projections $\mathbf{d}_i$ ($i = 1..M$) into four groups, representing the three orthogonal axes and the both diagonal marker. From each found line of four markers, we can infer the respective axis of the calibration object. We identify the lines by retrieving an approximation of the constant α from the X-ray image. Assuming $\mathbf{d}_1 \ldots \mathbf{d}_4$ are the four detected marker projections, classified as a line (ordered along that line), and $\mathbf{c}$ is the projection of the calibration object's origin $\mathbf{o}$ (symmedian point of the triangle bound by the three detected lines [1]), an approximation of α_j ($j \in \{x,y,z\}$) is given by:

$$\alpha_j = \frac{1}{2}\left(\frac{\alpha_j K_1}{K_1} + \frac{\alpha_j K_2}{K_2} \right) \approx \frac{1}{2}\left(\frac{\|\mathbf{d}_1 - \mathbf{c}\|}{\|\mathbf{d}_2 - \mathbf{c}\|} + \frac{\|\mathbf{d}_4 - \mathbf{c}\|}{\|\mathbf{d}_3 - \mathbf{c}\|} \right) \tag{4}$$

Using the value α_j obtained from (4), we can determine the corresponding axis of the marker projections. But we cannot infer the order of the markers in terms of direction nor can we assign both diagonal marker projections. Because each group is assigned in two ways (e.g. the projections of the markers on the x-axis: $\{(\mathbf{x}_1, \mathbf{d}_1), (\mathbf{x}_2, \mathbf{d}_2), (\mathbf{x}_3, \mathbf{d}_3), (\mathbf{x}_4, \mathbf{d}_4)\}$ and $\{(\mathbf{x}_1, \mathbf{d}_4), (\mathbf{x}_2, \mathbf{d}_3), (\mathbf{x}_3, \mathbf{d}_2), (\mathbf{x}_4, \mathbf{d}_1)\}$), we are considering 16 possible marker assignments.

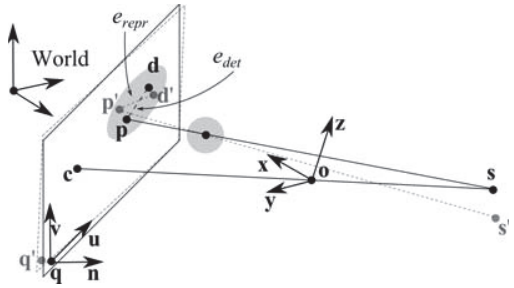

Fig. 4. The projection geometry: X-ray source position **s**, image position **q** and a calibration object at **o** with a ball marker. The X-ray projection of **o** is called **c**. The real image position of the projected marker center is **p**, the detected position is **d** (the difference of both is the detection error e_{det}). Position **p**' is the re-projection of the marker using the calibrated parameters **s**' and **q**' (the difference of **p**' and **d**' is the re-projection error e_{repr}).

D. Geometric parameter determination

We directly determine the geometric parameters for each possible marker assignment by solving a linear equation system as described in [1]. Each set of geometric parameters is verified using a score based on the re-projection errors $e_{repr,i}$ (fig. 4) of this configuration: mean μ_e, variance σ_e^2 and maximum e_{max}. Because of the unambiguity of the marker projections (imposed by the asymmetry constraint $K_1 \neq K_2$), the best score indicates the correct marker assignment and geometric parameter set.

In the last step we refine the geometric parameters using a non-linear Levenberg-Marquardt optimization algorithm to minimize the sum of squared re-projection errors e_{repr}. Because of the good initialization with the directly determined parameters, the optimization problem can be solved efficiently.

E. The degenerated cases

There are two basic problems that might occur when dealing with X-ray images of the marker arrangement described in section II A (for example fig. 5 right):

- Marker overlaps: two or more ball markers form an overlap in the image.
- Structural overlaps: two axes of markers form nearly the same line in the image.

The detection of marker overlaps is not fully possible by using features like size or intensities of detected regions (especially with oblique X-ray projections and elliptical marker regions). We recognize marker overlaps, if less than 14 regions were detected in the image. We then assume for each region that it is an overlap and divide all 14 markers accordingly into four groups (representing the three orthogonal and one diagonal axis). The respective marker centers $\mathbf{d}_i$ of an overlap are approximated by determining the center and the main axis of this region. All marker groups are verified by the following criteria:

- Each detected line must contain exactly the same number of marker projections on each side of **c**.
- We dissolve a structural overlap with eight marker projections, by verifying both identified lines using (4).
- There must be either none or two marker projections not assigned to any line ($\mathbf{s}_1$ and $\mathbf{s}_2$).

Fig. 5. Calibration object with 14 steel balls (left) and exemplary X-ray image of the calibration object with our CBCT system ORBIT (right).

- In case a marker projection is detected near **c**, we assume that the X-ray projection is in direction of an orthogonal or diagonal axis and these marker projections are ignored.

For each marker group in accordance with the criteria, we perform a marker assignment (section II C) and verify the resulting parameter set using the score function (section II D).

The approximated marker centers $\mathbf{d}_i$ of an overlap are only used for marker assignment and not for the determination of the geometric parameters.

III. Calibration Object

We constructed and manufactured a calibration object with 14 drill-holes to perform a geometric calibration of single X-ray projections images acquired with our open CBCT system. By the defined arrangement and depth of the drill-holes, 14 steel balls with 3 mm diameter can be placed accordingly to the previously described marker arrangement in section II A (Fig. 5 left). To verify and compensate manufacturing inaccuracies, we scanned the calibration object with an industrial CT and measured the exact steel ball locations. By taking arbitrary X-ray projections of this calibration object, the geometric parameters of each image can be determined using our proposed method (fig. 5 right).

IV. Results

At the current project state, the image detector of our open CBCT prototype is fixed on the patient table (fig. 1). Therefore, we first applied our calibration method on a scanning trajectory similar to tomosynthesis: a circularly moving X-ray source above an object on a fixed image detector (fig. 6).

A. Simulation results

Using our simulation environment, we generated 360 artificial projection images of our calibration object equally distributed along this scanning trajectory. The acquisition parameters were defined according to our open CBCT system setup: 298 x 298 mm² image size with 1024 x 1024 px and a distance from X-ray source to image center of approximately 1050 mm. The artificial images are ideal projections of our marker arrangement without noise or motion artifacts. We calculated the nine geometric parameters of all images and compared the results with the defined parameters of the

simulation environment. Additionally, we calculated the accuracy of our marker center detection algorithm (e_{det}) and the re-projection error of the calibrated configuration (e_{repr}). The results are shown in table 1.

TABLE I
SIMULATION RESULTS

		μ	σ	max
Marker detection error e_{det} [mm]		0.009	0.005	0.036
Image center position error [mm]	u	0.029	0.026	0.166
	v	0.033	0.035	0.239
	n	0.046	0.037	0.237
	∥	0.066	0.054	0.344
	⊥	0.004	0.002	0.015
X-ray source position error [mm]	u	0.634	0.548	3.375
	v	0.672	0.722	3.988
	n	0.940	0.770	3.954
	∥	1.375	1.110	5.680
	⊥	0.136	0.104	0.554
Image orientation error [°]	η	0.004	0.004	0.022
	θ	0.005	0.005	0.027
	φ	0.006	0.004	0.040
Re-projection error e_{repr} [mm]		0.008	0.005	0.038

The image center and source position errors are given in image coordinate system **u-v-n**. The symbols ∥ and ⊥ indicate position deviations in direction (∥) and perpendicular (⊥) to the central X-ray beam. The angles η, θ, and φ describe the image rotation errors in **uv**-, **vn**- and **un**-plane of the image coordinate system.

B. Experimental results

Furthermore, we applied the calibration method on the open CBCT prototype and acquired 360 images of our calibration object. We calculated the geometric parameters of each acquired image and repeated the scanning trajectory with vertebral bodies of the lumbar spine. Based on the calculated geometric parameters and the 360 projection images, we reconstructed the scanned volume with a simultaneous algebraic reconstruction technique. Fig. 6 shows the vertebral test bodies and an axial and coronal slice of the reconstructed volume. As a quantitative measurement of the experimental result, we calculated the re-projection errors $e_{repr,i}$ using the calibrated parameters and the found marker assignment of each image of the calibration object: $\mu = 0.058$ mm, $\sigma = 0.047$ mm, $e_{max} = 0.583$ mm.

V. CONCLUSION AND DISCUSSION

The errors in the simulation (shown in table I) result from the marker center detection of the projected ball markers and the parameter determination with our calibration method. Discrepancies between the real and calibrated geometric parameters mainly occur in direction of the projection (indicated with symbol ∥ in table I), but these deviations have little impact on the accuracy of the x-ray projections. Regarding the image plane, the maximum error of the image center position is less than a pixel size of 0.29 mm.

By applying our method on the open CBCT system, additional errors influence the resulting accuracy: the repeatability of the X-ray source positioning by the robot-arm and inaccuracies of the manufactured calibration body. Errors caused by the movement of the X-ray source during the image acquisition are excluded at the moment, as the image acquisition is currently done in defined fixed positions. In further project work we will develop a motorized mechanism to move the flat-panel detector independently of the X-ray source and execute freely definable scanning trajectories. To compensate occurring mechanical instabilities, we will perform an additional online calibration method during the image acquisition.

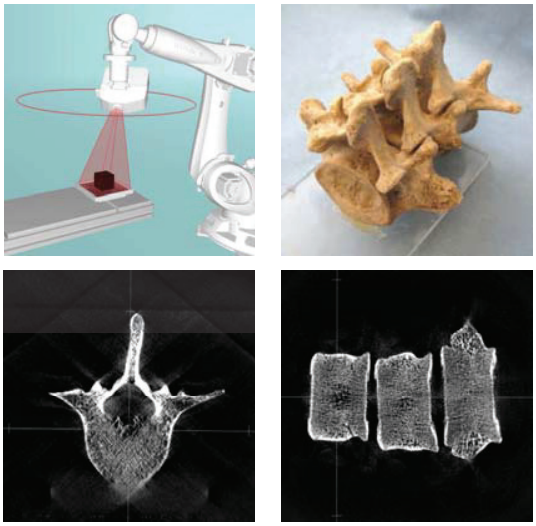

Fig. 6. a) Executed and calibrated scanning trajectory with a fixed flat-panel detector; b) Vertebral bodies of the lumbar spine; c) Axial slice of the reconstructed volume; d) Coronal slice of the reconstructed volume.

REFERENCES

[1] C. Mennessier, R. Clackdoyle, and F. Noo, "Direct determination of geometric alignment parameters for cone-beam scanners.," *Physics in medicine and biology*, vol. 54, no. 6, pp. 1633–60, Mar. 2009.

[2] Y. Cho, D. J. Moseley, J. H. Siewerdsen, and D. a. Jaffray, "Accurate technique for complete geometric calibration of cone-beam computed tomography systems," *Medical Physics*, vol. 32, no. 4, p. 968, 2005.

[3] K. Yang, A. L. C. Kwan, and D. F. Miller, "A geometric calibration method for cone beam CT systems," *Med Phys.*, vol. 33, no. 6, pp. 1695–1706, 2006.

[4] J. C. Ford, D. Zheng, and J. F. Williamson, "Estimation of CT cone-beam geometry using a novel method insensitive to phantom fabrication inaccuracy: Implications for isocenter localization accuracy," *Medical Physics*, vol. 38, no. 6, p. 2829, 2011.

[5] M. J. Daly, J. H. Siewerdsen, Y. B. Cho, D. a. Jaffray, and J. C. Irish, "Geometric calibration of a mobile C-arm for intraoperative cone-beam CT," *Medical Physics*, vol. 35, no. 5, p. 2124, 2008.

[6] X. Wang, J. G. Mainprize, M. P. Kempston, G. E. Mawdsley, and M. J. Yaffe, "Digital breast tomosynthesis geometry calibration," *Proceedings of SPIE*, vol. 6510, p. 65103B–65103B–11, 2007.

[7] S. Johnston, G. Johnson, and C. Badea, "Geometric calibration for a dual tube/detector micro-CT system," *Medical Physics*, vol. 35, no. 5, pp. 1820–1829, 2008.

[8] N. Robert, K. N. Watt, X. Wang, and J. G. Mainprize, "The geometric calibration of cone-beam systems with arbitrary geometry.," *Physics in medicine and biology*, vol. 54, no. 24, pp. 7239–61, Dec. 2009.

[9] C. Mennessier, B. Spencer, R. Clackdoyle, and T. Xu, "Distortion correction, geometric calibration, and volume reconstruction for an isocentric C-Arm X-Ray system," *(NSS/MIC), 2011*, pp. 2943–2947, 2011.

[10] R. Clackdoyle and C. Mennessier, "Centers and centroids of the cone-beam projection of a ball.," *Physics in medicine and biology*, vol. 56, no. 23, pp. 7371–91, Dec. 2011.